

ARTICLE

OPEN

Attribution of late summer early autumn Arctic sea ice decline in recent decades

Lejiang Yu¹✉, Shiyuan Zhong², Timo Vihma³ and Bo Sun¹

The underlying mechanisms for Arctic sea ice decline can be categorized as those directly related to changes in atmospheric circulations (often referred to as dynamic mechanisms) and the rest (broadly characterized as thermodynamic processes). An attribution analysis based on the self-organizing maps (SOM) method is performed to determine the relative contributions from these two types of mechanisms to the Arctic sea ice decline in August–October during 1979–2016. The daily atmospheric circulations represented by daily 500-hPa geopotential height anomalies are classified into 12 SOM patterns, which portray the spatial structures of the Arctic Oscillation and Arctic Dipole, and their transitions. Due to the counterbalance between the opposite trends among the circulation patterns, the net effect of circulation changes is small, explaining only 1.6% of the declining trend in the number of August–October sea ice days in the Arctic during 1979–2016. The majority of the trend (95.8%) is accounted for by changes in thermodynamic processes not directly related to changes in circulations, whereas for the remaining trend (2.6%) the contributions of circulation and non-circulation changes cannot be distinguished. The sea ice decline is closely associated with surface air temperature increase, which is related to increasing trends in atmospheric water vapor content, downward longwave radiation, and sea surface temperatures over the open ocean, as well as to decreasing trends in surface albedo. An analogous SOM analysis extending seasonal coverage to spring (April–October) for the same period supports the dominating role of thermodynamic forcing in decadal-scale Arctic sea ice loss.

npj Climate and Atmospheric Science (2021)4:3; <https://doi.org/10.1038/s41612-020-00157-4>

INTRODUCTION

Observations in the Arctic Ocean have shown a rapid decline in sea ice extent especially in recent decades¹. This decline has been attributed in part to the warming of the global climate associated with increasing greenhouse gas emissions^{2–4}; the warming rate over the Arctic is nearly twice the global average⁵. However, the predicted rates of sea ice retreat by general circulation models (GCM) under various greenhouse gas emissions scenarios have been, in general, smaller than the observed rates⁶, indicating that other mechanisms may have also played a role. One such mechanism is changes in aerosol emissions that, through aerosol-radiation feedback, can contribute to Arctic sea ice loss^{7,8}.

Another major factor for Arctic sea ice loss is changes in the atmospheric and oceanic circulation that can alter the trajectory, and rate of transport of heat and moisture into the Arctic Ocean^{9–16}. Studies have revealed a connection between the main modes of atmospheric circulation in the mid-high latitudes and the modes of Arctic sea ice variations. For example, an upward trend in the North Atlantic Oscillation⁹, the Arctic Oscillation (AO)¹⁰, and the Arctic Dipole (AD)¹¹ indices has been linked to a downward trend in the Arctic sea ice extent. Atmospheric and oceanic variability modes on decadal to multidecadal scales, such as the Pacific Decadal Oscillation¹⁷ and the Atlantic Multidecadal oscillation (AMO)¹⁸, have also been linked to the variability in the Arctic sea ice cover^{12–16}. However, the extent to which the atmospheric and oceanic variability modes have influenced the Arctic sea ice loss remains an open question. Estimates of the internal variability from GCMs vary significantly, between 20 and 50% (refs. ^{19–21}), and large discrepancies exist between the observed and GCM-simulated sea ice concentrations^{22–24} due possibly to a

combination of factors, including low sea ice sensitivity to greenhouse gas emissions²⁵, errors, and uncertainties in sea ice and atmospheric models, and inadequate treatment of sea ice-atmosphere interactions^{26,27}.

Previous studies have investigated the Arctic sea ice loss from the perspectives of changes in atmospheric and oceanic circulation patterns, also known as dynamic forcing, and non-circulation-related changes broadly referred to as thermodynamic processes, but the relative contributions of the two types of drivers to the Arctic sea ice retreat have not been well quantified. While some studies have stressed the dominating role of thermodynamic forcing on the Arctic sea ice decline^{4,28,29}, others have demonstrated important dynamical effects^{30–33}. The aim of our study is to statistically assess the relative contributions to the August–October Arctic sea ice loss over the 1979–2016 period from changes in atmospheric circulations (dynamic forcing) and those not directly related to circulations (thermodynamic forcing). We also determine what circulation patterns make large contributions to Arctic sea ice loss and how these patterns relate to known atmospheric modes in the northern high latitudes. This is accomplished by utilizing the self-organizing maps (SOM) method³⁴ to extract the August–October main atmospheric variability modes. As a well-established statistical method for pattern recognition, the SOM method has been widely used in climate science; however, to our knowledge, it has not been applied to the decomposition of atmospheric circulations to explain Arctic sea ice decline. Our analyses focus on late summer and early fall (August–October) to capture the time of minimum sea ice extent that usually occurs in September. Refer to the “Dataset” and “Methods” sections for a detailed description of the SOM method and how it is utilized for this analysis.

¹State Oceanic Administration Key Laboratory for Polar Science, Polar Research Institute of China, Shanghai, China. ²Department of Geography, Environment and Spatial Sciences, Michigan State University, East Lansing, MI, USA. ³Finnish Meteorological Institute, Helsinki, Finland. [✉]email: yulejiang@sina.com.cn

RESULTS

SOM analysis of 500-hPa geophysical height

We first analyze trends in sea ice extent over the Arctic Ocean north of 60° latitude. The number of August–October days with sea ice present, defined as when sea ice occupies at least 15% of a $25 \text{ km} \times 25 \text{ km}$ grid cell, is calculated for each year over the 1979–2016 period and the average number over the 38-year period along with the linear trend are shown in Fig. 1. On average, the numbers are larger (>70 days) over the central Arctic Ocean, decreasing to <10 days (Fig. 1a) over the Barents and Chukchi Seas, southern Kara Sea, and Baffin Bay. The numbers exhibit a significant downward trend nearly everywhere, and the strongest trend ($\sim 2 \text{ days yr}^{-1}$) is over the marginal seas particularly the

Kara, East Siberian, and Chukchi Seas (Fig. 1b). The downward trend in the number of days with August–October sea ice present in Arctic Ocean is consistent with the trend in the sea ice concentration (not shown) for the same period.

To understand how much the sea ice trends can be explained by changes in atmospheric circulations, we next examine the corresponding large-scale circulation patterns, represented by the 500-hPa geopotential height fields, for the same period. Using SOM, we classify the August–October anomalous daily atmospheric circulation patterns during 1979–2016 into a 4×3 SOM grid or 12 SOM nodes/patterns. Each August–October day during the 38 years is mapped onto 1 of the 12 nodes based on minimum Euclidean distance (Fig. 2). The 12 SOM spatial patterns depict a smooth transition between negative and positive phases of the AO (nodes 5 and 8, respectively) and dipole states (the other nodes). The dipole pattern, with a negative anomaly of $>100 \text{ gpm}$ over the eastern Arctic Ocean (node 12), has the largest (13.7%) mean annual frequency of occurrence (calculated as the number of daily 500 hPa height anomaly patterns best represented by the node divided by the total August–October days each year, averaged over 38 years), while its opposite spatial pattern (node 1) has the third largest (12.1%) mean annual frequency of occurrence. The frequency of occurrence of node 12 exhibits a decadal variability with an average occurrence of 17.1 days per year prior to 1996 and 9.3 after it (Fig. 3), but the decadal variability signal is absent from the time series of occurrence for node 1. Nodes 9 and 4 has a spatial pattern that nearly mirrors each other, but node 9 has the second-highest mean

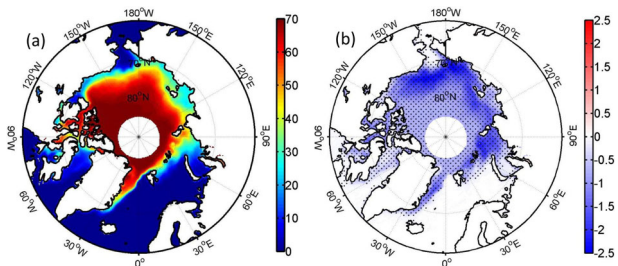


Fig. 1 The climatology (units: day) (a) and trend (units: day yr^{-1}) (b).

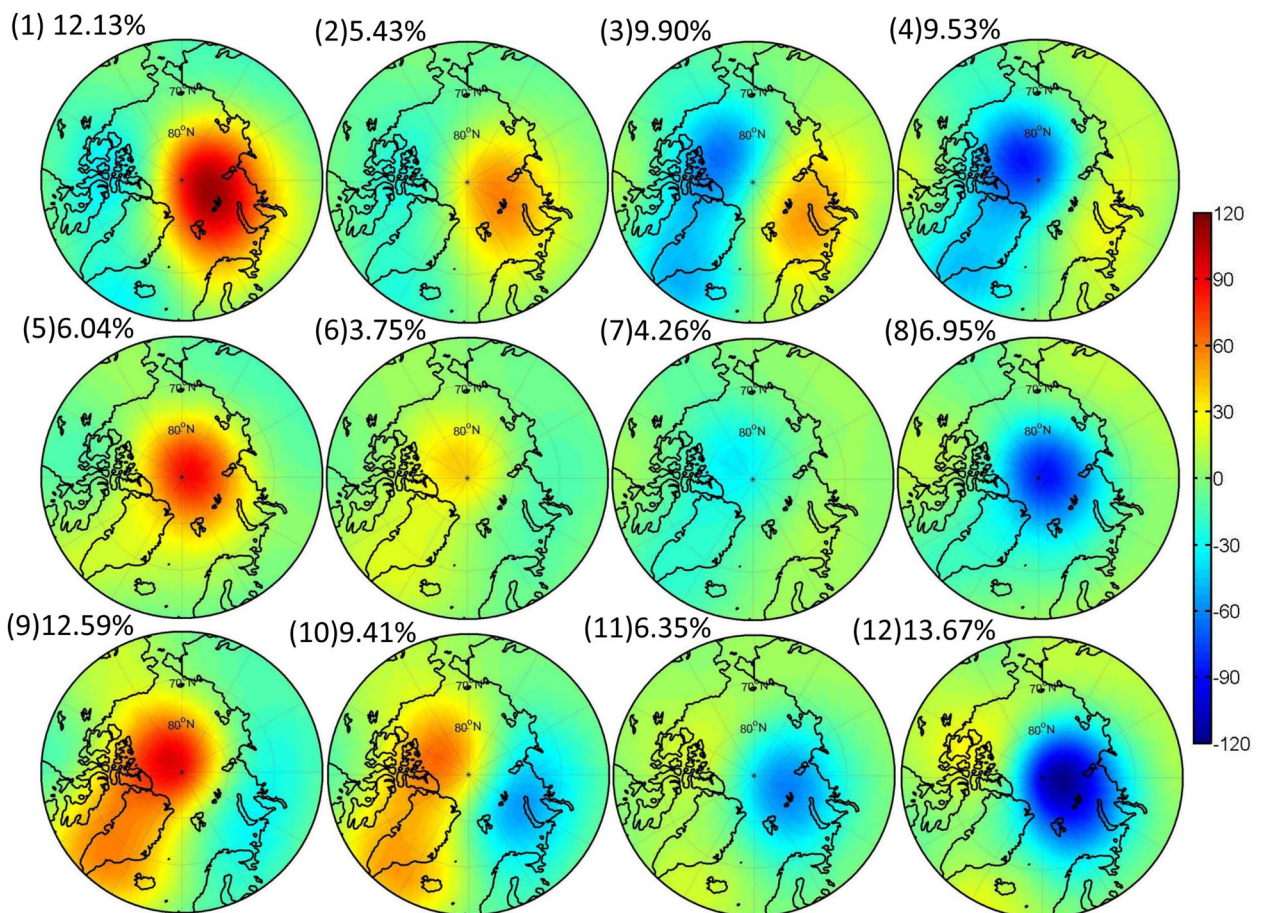


Fig. 2 SOM patterns of August–October daily 500-hPa geopotential height anomalies (units: gpm) on a 4×3 SOM grid for the 1979–2016 period. The percentages at the top left of each panel indicate the frequency of occurrence of the pattern.

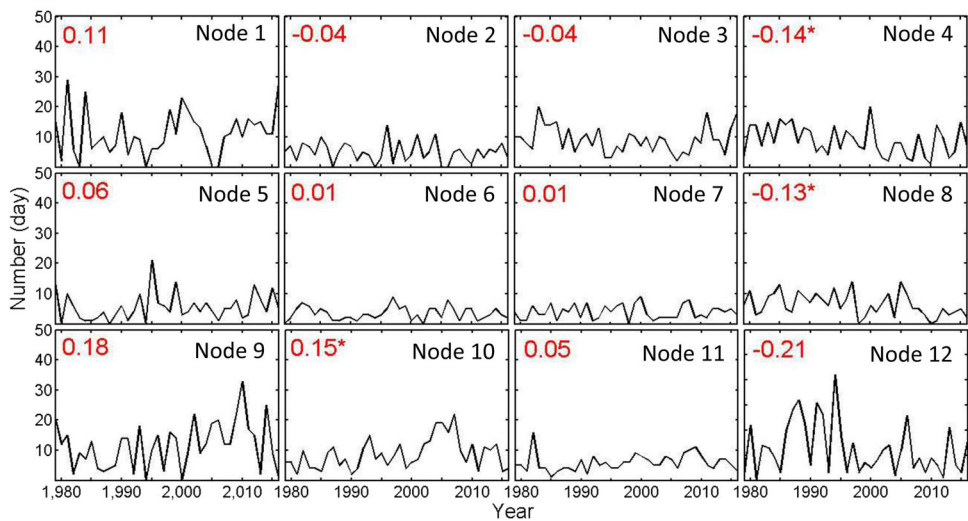


Fig. 3 Time series of occurrence number and its trend (red numbers, in day yr^{-1}) for each SOM pattern in Fig. 2. Red asterisks indicate the trends significant at 95% confidence level.

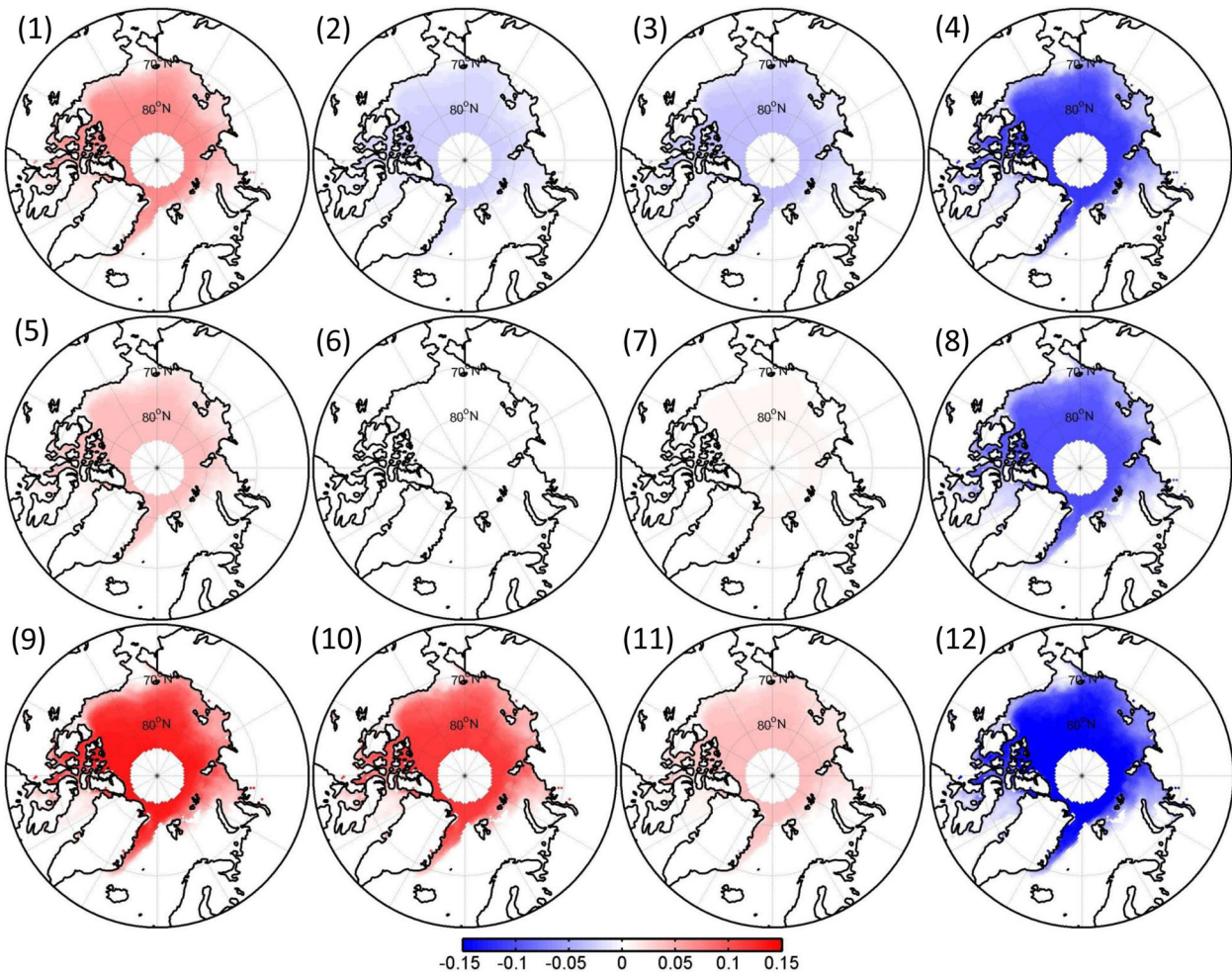


Fig. 4 Contribution from the dynamic components to the trends in the number of August–October Arctic sea ice days for each of the 12 SOM nodes (units: day yr^{-1}).

annual frequency of 12.6%, while node 4 occurs at lower frequency of 9.5%.

The annual frequency of occurrence of each SOM node displays a significant interannual variability and some also exhibits a linear trend (Fig. 3). Node 9 has the sharpest, but insignificant trend, while node 4 has a significant decreasing trend. Nodes 3 and 10 have opposite but comparable height anomalies over the eastern and western Arctic, with a similar occurrence frequency of 9.9% and 9.4%, respectively. The significant positive trend in the occurrence time series of node 10 (Fig. 3) indicates increasing (decreasing) occurrence of positive height anomalies over western (eastern) Arctic. Positive (negative) height anomalies prevail over the Arctic Ocean for node 5 (node 8). The occurrence of node 8 displays a significant negative trend, while no significant trend is detected for node 5 (Fig. 3).

Dynamic, thermodynamic, and interaction components

Below, we investigate the contribution from each node to the total trend in the number of August–October sea ice days in terms of dynamic (circulation related), thermodynamic (non-circulation related), and so-called interaction components as described by Eq. (2) in the “Dataset” and “Method” section. The contribution from the dynamic component for each node is shown in Fig. 4 and Table 1. For each node, the trend contributed by the dynamic component is consistent in direction everywhere, and decreases

Table 1. The domain-averaged trends of the number of days with sea ice concentration ≥ 0.15 for dynamic, thermodynamic, and interaction components of each node and their total trends.

Node	Dynamic Trend	Thermodynamic Trend	Interaction Trend	Total Trend
1	0.029	-0.054	-0.015	-0.039
2	-0.010	-0.040	-0.007	-0.058
3	-0.014	-0.070	-0.021	-0.105
4	-0.048	-0.068	-0.004	-0.120
5	0.017	-0.016	-0.009	-0.008
6	0.002	-0.018	-0.006	-0.022
7	0.003	-0.036	0.002	-0.031
8	-0.044	-0.060	0.012	-0.092
9	0.056	-0.077	0.019	-0.002
10	0.049	-0.069	0.006	-0.014
11	0.017	-0.043	-0.007	-0.033
12	-0.067	-0.077	0.012	-0.132
Total	-0.010	-0.628	-0.017	-0.656

Units are day yr^{-1} .

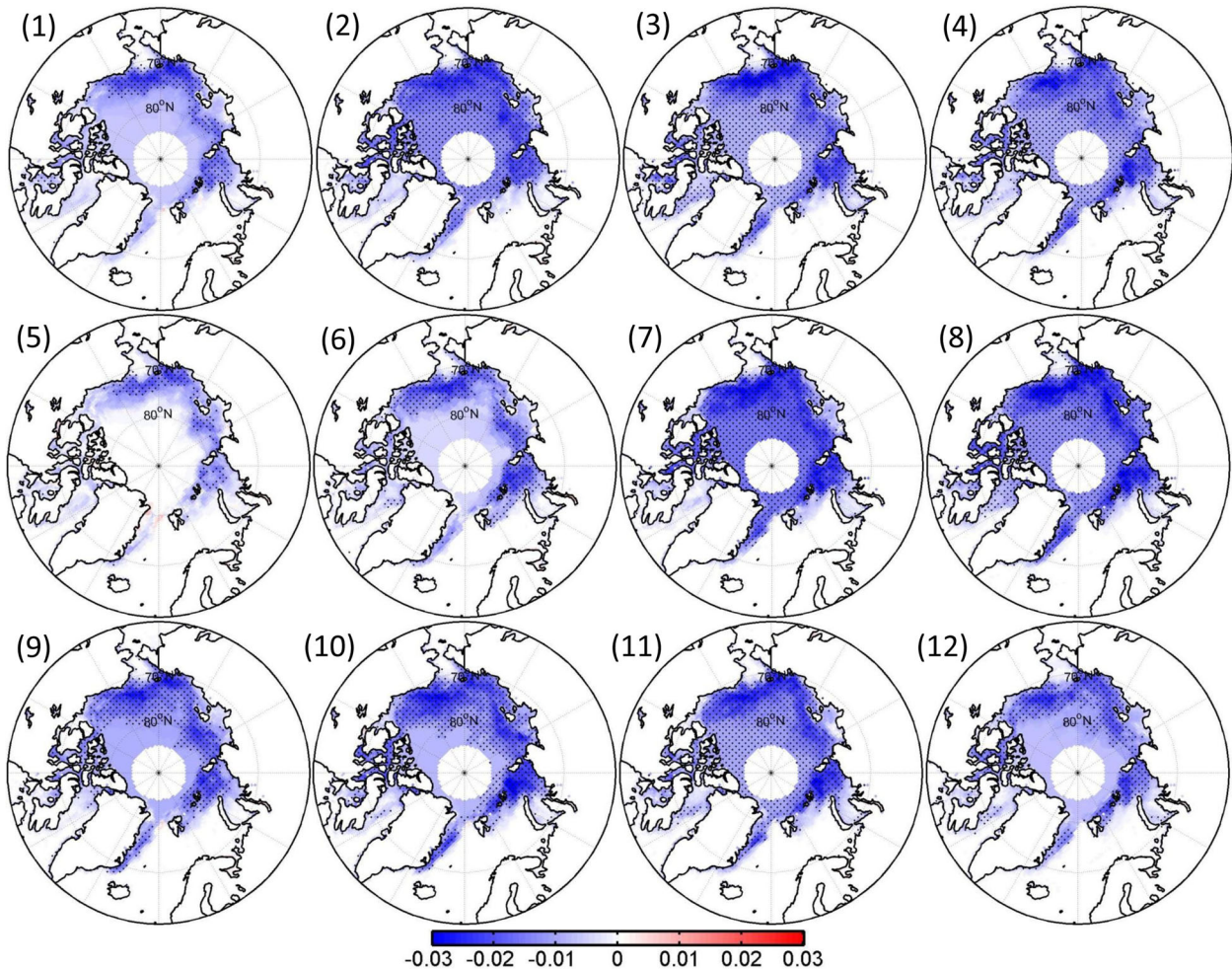
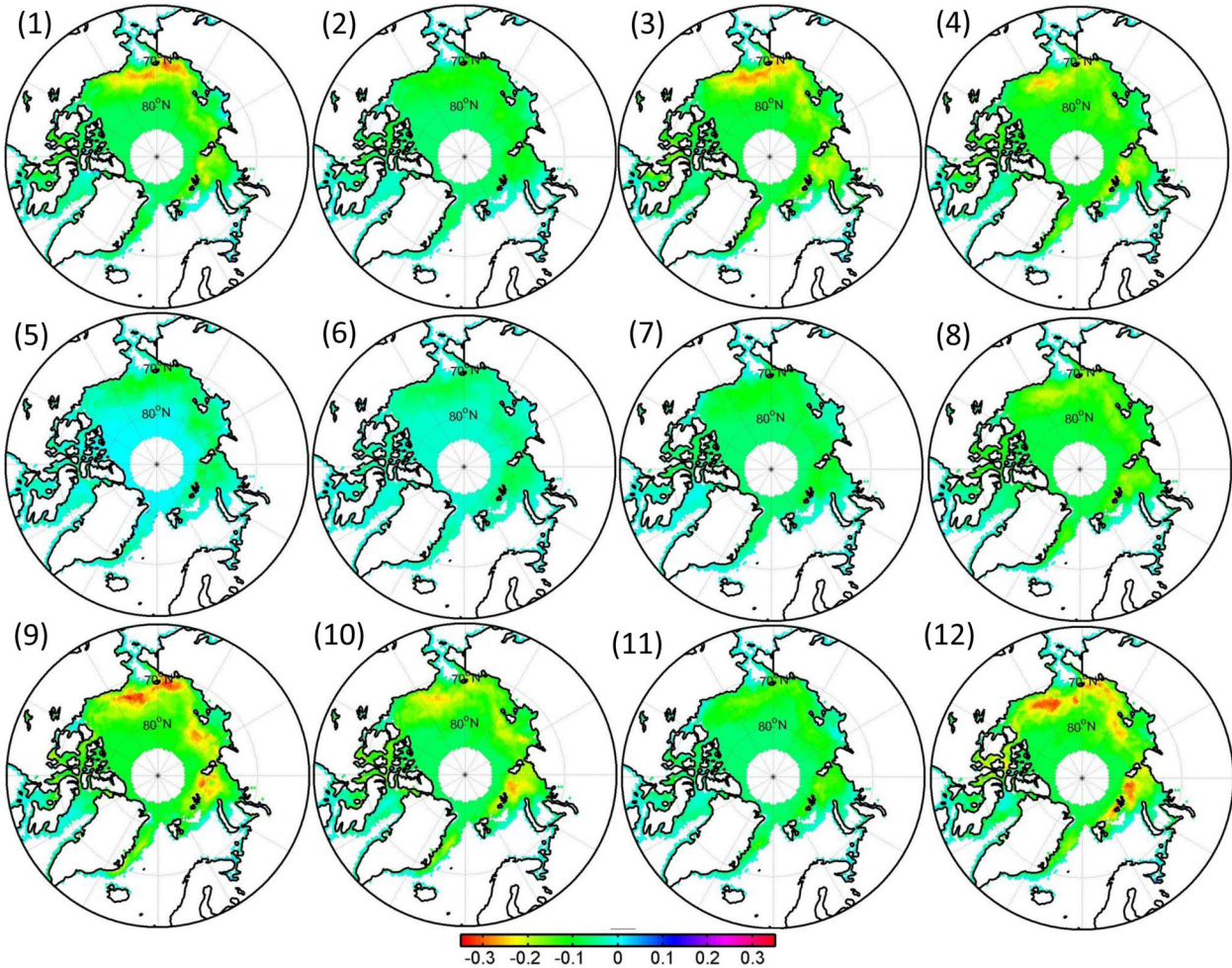


Fig. 5 Trends in the percentage of August–October Arctic sea ice presence per each SOM node occurrence (units: yr^{-1}).

Table 2. The domain-averaged trends in the sea ice days per the node occurrence.

Node 1	Node 2	Node 3	Node 4	Node 5	Node 6	Node 7	Node 8	Node 9	Node 10	Node 11	Node 12
Trend	-0.002	-0.003	-0.002	-0.002	-0.001	-0.002	-0.003	-0.003	-0.002	-0.002	-0.002

Units are yr^{-1} .

**Fig. 6** Contribution from the thermodynamic components to the trends in the number of August–October Arctic sea ice days for each of the 12 SOM nodes (units: day yr^{-1}).

slowly in magnitude from the central Arctic Ocean toward the marginal seas. For each SOM node, the magnitude of the dynamic component depends on the trend in the occurrence of the SOM node and on the climatological frequency of sea ice occurrence for the node (Eq. (2)). The most negative dynamic trend occurs for node 12 ($-0.067 \text{ days yr}^{-1}$), followed by node 4 ($-0.048 \text{ days yr}^{-1}$) and node 8 ($-0.044 \text{ days yr}^{-1}$). The spatial patterns of these nodes are similar to the positive phase of the AO index, with average daily index values of 0.7, 0.7, and 0.6 for nodes 4, 8, and 12, respectively. The positive phase of the AO index is favorable for a decreasing surface temperature and increasing sea ice concentration in the Arctic^{10,35}. These three nodes have large negative trends in their occurrences leading to a negative dynamic component for sea ice occurrence. Node 9 has the most positive dynamic trend with a domain-averaged value of $0.056 \text{ days yr}^{-1}$,

followed by node 10 ($0.049 \text{ days yr}^{-1}$). The two nodes have large positive trends in their occurrences, though the trend for node 9 is below the 95% confidence level. The spatial patterns of the two nodes are similar to the positive phase of the AD, which is associated with cold air flow from the central Arctic and an increase in sea ice extent due to southward transport of ice^{11,36}. Accordingly, nodes 9 and 10 yield positive dynamic contribution to sea ice occurrence.

For each node, the thermodynamic component depends on the change in the number of sea ice days accompanying the node and the average frequency of node occurrence (Eq. (2)). The former controls the sign of the thermodynamic contribution. For all nodes, sea ice days during the node occurrences exhibit a downward trend everywhere in the domain (Fig. 5 and Table 2). Nodes 7 and 8 have the strongest negative trends ($-0.003 \text{ days yr}^{-1}$) in the

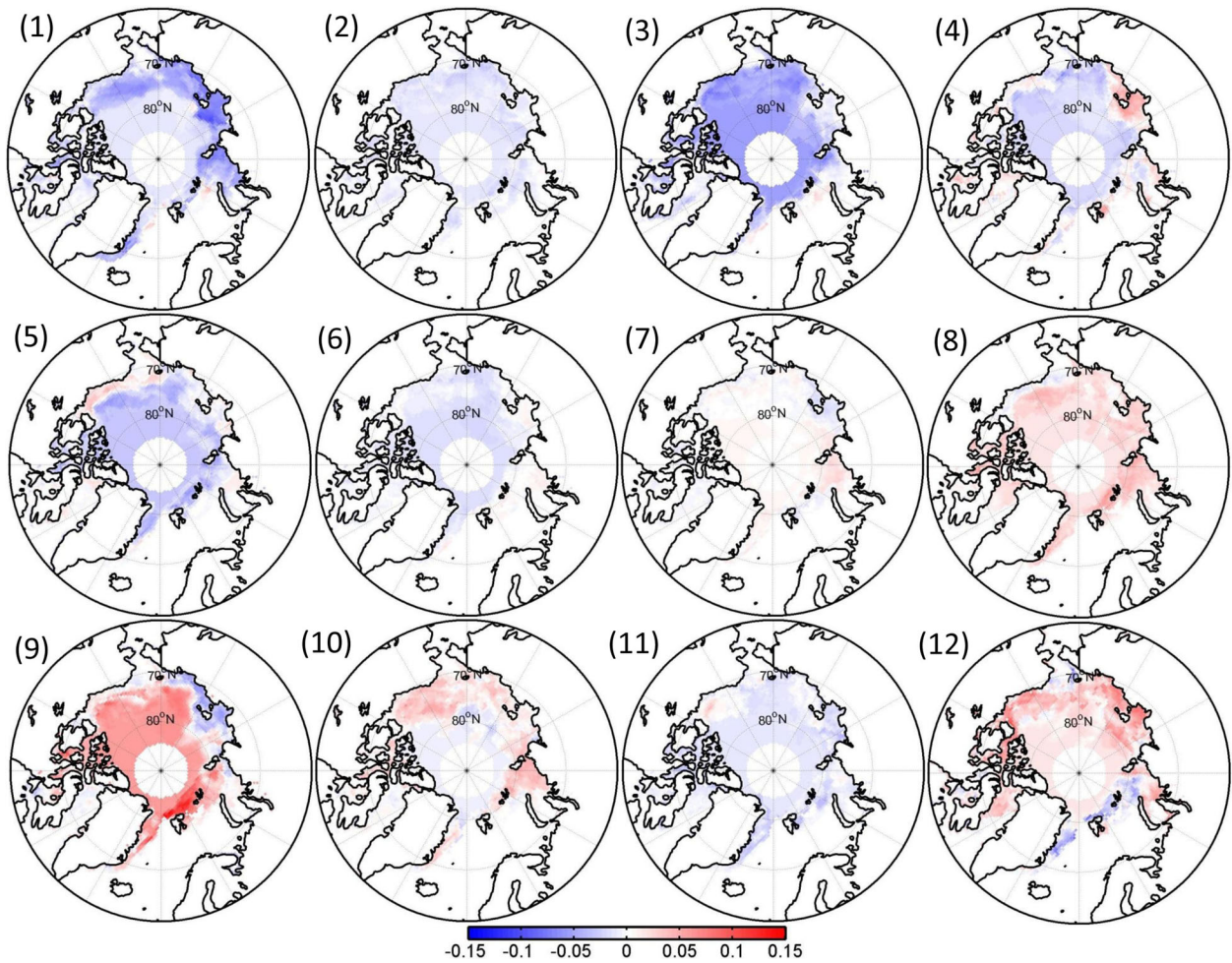


Fig. 7 Contribution from the interaction components to the trends in the number of August–October Arctic sea ice days for each of the 12 SOM nodes (units: day yr^{-1}).

corresponding sea ice days, although they have spatial patterns unfavorable for Arctic sea ice decrease. In contrast, node 5 has the weakest negative trend ($-0.001 \text{ days yr}^{-1}$) in the corresponding sea ice days. It is not surprising that the thermodynamic component is favorable for the Arctic sea ice retreat for all nodes (Fig. 6). Large sea ice loss occurs mainly over the Chukchi, East Siberian, Barents, and Kara seas. The thermodynamic contribution varies considerably among the nodes. The largest contributions are from nodes 9 to 12, with domain-averaged trend of $-0.077 \text{ days yr}^{-1}$ (Table 1). In contrast to node 9 for which the contributions from the dynamic and thermodynamic components counterbalance each other, node 12 has the contributions from the two components superimpose on each other. Node 5 has the smallest domain-averaged thermodynamic contribution of $-0.016 \text{ days yr}^{-1}$. We note that the frequency of SOM nodes is closely linked to the thermodynamic components with correlation coefficient of -0.83 , i.e., the sea ice occurrence has decreased most rapidly for the most frequently occurring SOM nodes. Besides the different magnitude, the thermodynamic components vary in spatial patterns (Fig. 6). For nodes 1, 2, 3, and 5, the sea ice loss in the Pacific sector produced by the thermodynamic contributions is noticeably larger than that in the Atlantic sector. For other nodes, the sea ice loss is comparable in the Atlantic and Pacific sectors.

The magnitude of the so-called interaction components is smaller than those of the thermodynamic components, but larger than those of the dynamic components (Fig. 7). For most nodes, in

particular 4, 5, 9 and 12, the signal of the interaction component shows a spatially nonuniform change. Node 9 generates the largest domain-averaged interaction component for the trend in sea ice days ($0.019 \text{ days yr}^{-1}$), followed by node 8 ($0.012 \text{ days yr}^{-1}$), while node 3 has the largest negative interaction component of $-0.021 \text{ days yr}^{-1}$ (Table 1). However, despite of its name the interaction component is often associated with random variations rather than interaction of physical processes³⁷. Hence, we do not pay particular attention to it.

Total contribution from three components

After separating the contributions from each of the three components to the trends in the August–October sea ice days for each node, we now move on to quantify the total contribution from all three components for each node (Fig. 8 and Table 1). For most nodes, the collective contribution from the three components accounts for negative trends over the entire study region, with the exception of nodes 5, 9, and 10 that have positive trends over the central Arctic and Canadian Arctic archipelago. With a domain-averaged trend of $-0.132 \text{ days yr}^{-1}$, node 12 contributes the most to the negative sea ice trend, which is followed by node 4 and then 3, with comparable dynamic and thermodynamic components. The smallest overall contribution is from node 9 because its negative thermodynamic component, although the

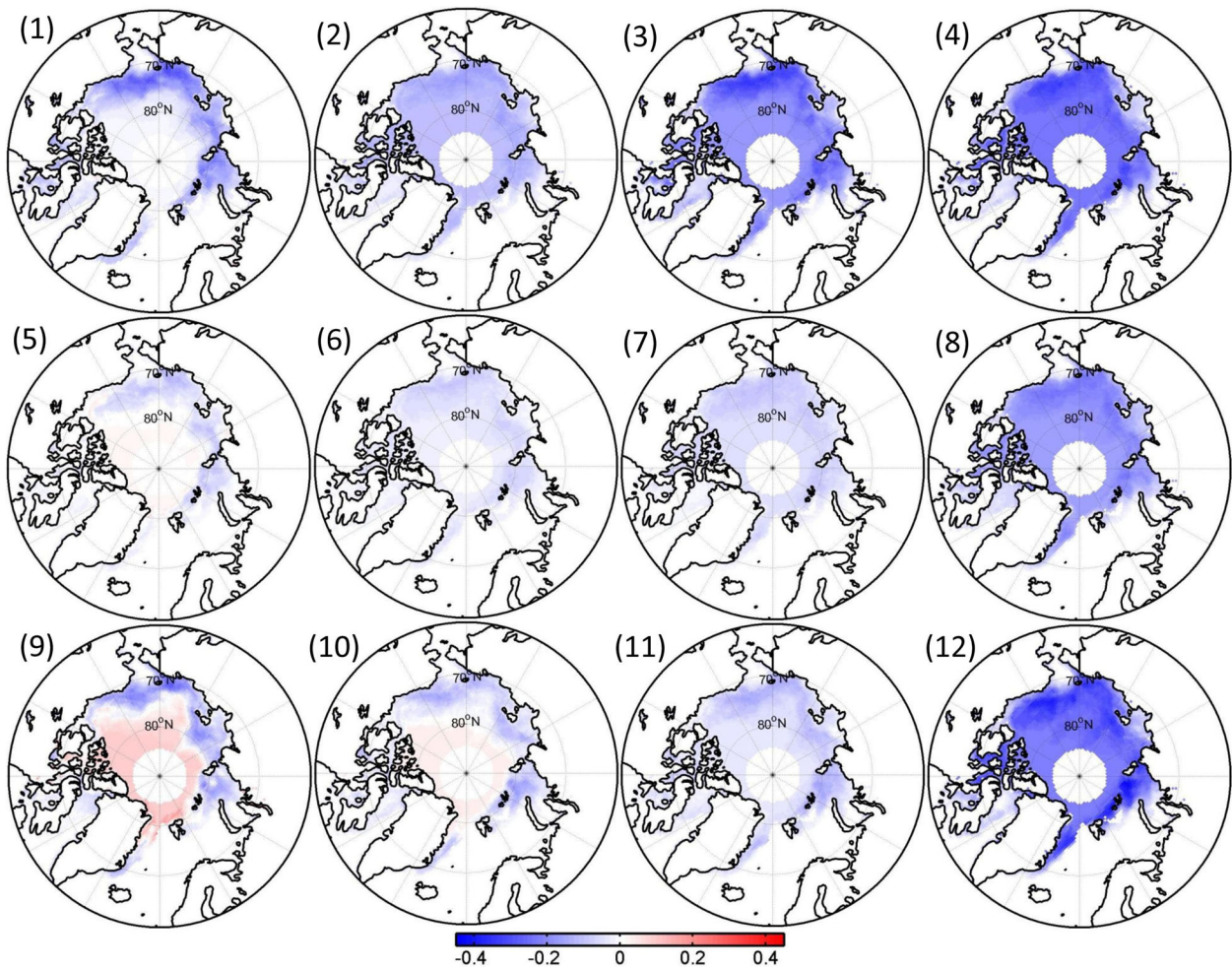


Fig. 8 Combined contribution from the dynamic, thermodynamic, and interaction components to the total trends in the August–October sea ice days from each of the 12 SOM nodes (units: day yr^{-1}).

largest among all nodes, is largely offset by the positive dynamic and interaction components.

Finally, we examine how each of the three components when summed over all 12 nodes contributes to the spatial variation of the trends in the August–October sea ice days (Fig. 9). The thermodynamic components that are consistent in sign and spatial distribution across all 12 nodes (Fig. 6) yield a pattern of total trend that is similar to that of individual nodes (Figs. 9a and 1b). The domain-averaged trend from the thermodynamic component is $-0.628 \text{ days yr}^{-1}$, which explains 95.8% of the total domain-averaged trend of $-0.656 \text{ days yr}^{-1}$. The collective dynamic trends are negative in most of the study region except for small parts of the Laptev, Barents, and Kara seas. Due to the offsetting effect among the nodes, the domain-averaged trend from the dynamic component is only $-0.010 \text{ days yr}^{-1}$, which explains 1.6% of the total trend. The remaining 2.6% of the total trend is explained by the so-called interactive component that, when summed over all 12 nodes, has a domain-averaged trend of $0.017 \text{ days yr}^{-1}$.

The results above indicate that thermodynamic components make the largest contributions to Arctic sea ice loss. According to Eq. (2), the thermodynamic component is related to the trend in the sea ice days, while holding circulation patterns unchanged over the study period. In other words, it is the part of the trend caused by factors unrelated to circulation pattern changes. The

thermodynamic components may include, among others, (i) Arctic warming associated with increasing greenhouse gas concentrations, (ii) decadal variability (e.g., due to AMO), (iii) changes in heat transport not associated with changes in circulation patterns, but with changes in other fields, such as upstream sea surface temperatures (SST), and (iv) changes in sea ice transport induced by changes in the gradient of sea ice concentration. We examine the changes in Arctic surface air temperature related to each node. There are a variety of Arctic feedbacks amplifying the global warming. Here, we focus on changes in water vapor, downward longwave radiation and surface albedo, and how they are related to increases in surface air temperature for each node. We first calculate the August–October average of anomalies in the daily surface air temperature, downward longwave radiation, and total column water vapor accompanying each node for each year, and then fit a linear trend to the average over the study period. Trends in these variables are shown for each node in Figs. 10–12. The surface air temperature has increased over the Arctic Ocean (Fig. 10), and the trends are consistent with those in the decreased number of days with sea ice present (Fig. 6). The regions with significant trends are distributed in the marginal seas. We compared spatial patterns of surface air temperature with those of the thermodynamic components through the spatial correlations between them for each node (Fig. 6). The results are shown at Table 3. All correlation coefficients are negative with values >0.5 .

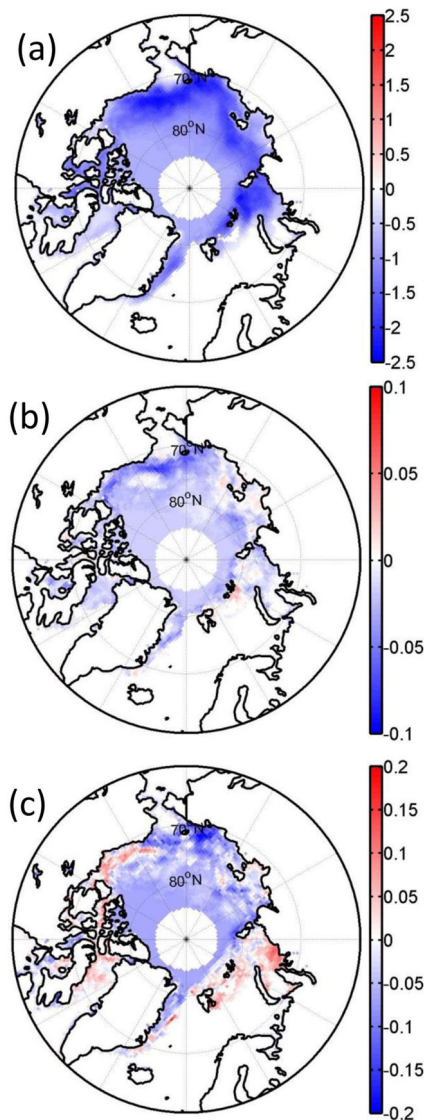


Fig. 9 The thermodynamic (a), dynamic (b), and interaction (c) contribution to total trends in the August–October Arctic sea ice days from all 12 SOM nodes (units: day yr^{-1}).

with the above 99% confidence level. The negative correlations for nodes 1, 5, 6, and 8 have magnitude >0.7 , indicating that majority of the spatial variability of thermodynamic components is statistically related to that of the trends in surface air temperature. The weakest negative correlations of -0.51 occur in nodes 3 and 4, indicating only 25% of the spatial variability of thermodynamic components explained by the variability in the surface air temperature trends. Also the trends in downward longwave radiation are positive for each node over the Arctic Ocean (Fig. 11). The downward longwave radiation depends above all on clouds and water vapor. Figure 12 shows an increasing total column water vapor over the Arctic Ocean for most of the nodes, suggesting a contribution of the water vapor feedback mechanism. Decreasing albedo in the region from Svalbard eastward to Beaufort Sea (Fig. 13) corresponds to increasing net solar radiation in the same regions (not shown), although downward solar radiation displays a decreasing trend across the Arctic Ocean (not shown). It indicates that albedo feedback contributes to thermodynamic components. Significantly, positive SST trends are distributed over all the marginal seas (Fig. 14). These positive

trends may result in an increasing meridional gradient in near-surface air temperature, which leads to heat transport toward the North Pole with the aid of climatological southerly wind (which does not require any circulation change), thus contributing to thermodynamic components.

Given the influence of springtime atmospheric circulation on summertime Arctic sea ice, we extend our analysis into the April–October period. The SOM decomposition of the daily April–October 500-hPa geopotential height anomalies show spatial patterns (Supplementary Fig. 1) that closely resemble those of the August–October patterns (Fig. 2). The dynamic, interaction, and thermodynamic components contributed to -0.9 , -6.8 , and 107.7% of the total April–October sea ice trends, respectively. The thermodynamic components for the 12 nodes (Supplementary Fig. 2) show negative trends across the Arctic Ocean, especially in its marginal seas, which is similar to the thermodynamic components for the August–October period. However, some spatial patterns are different from those of the August–October period. For nodes 1, 2, and 3, the sea ice loss in the Pacific and Atlantic sectors are comparable for April–October, but for August–October the losses are larger in the Pacific Sector. For nodes 4, 5, 6, 9, and 10, the negative trends are more remarkable in the Atlantic than the Pacific sector for April–October, which is not the case for August–October. These differences suggest seasonal influences on the thermodynamic components. In addition, unlike the August–October analysis, the frequency of the SOM nodes is not significantly associated with the thermodynamic component in the April–October analysis.

DISCUSSION

In this study, the SOM method is utilized to statistically estimate the contributions to the declining trends in the August–October Arctic sea ice cover over the 1979–2016 period from changes in large-scale atmospheric circulations known as dynamic forcing and in other mechanisms not directly related to circulations that are broadly categorized as thermodynamic forcing.

Among the 12 SOM nodes used to classify the anomalous daily atmospheric circulation patterns during the study period, nodes 4 and 8, characterized by negative 500-hPa height anomalies over most of the Arctic, show a significantly decreasing trend in their occurrence over the 38-year period. In contrast, node 10, with positive (negative) height anomalies over the western (eastern) Arctic, has an increasing trend. Because of the opposite trends among the circulation patterns, the collective contribution from the changes in circulations or the dynamic component to the decreasing trend of the August–October Arctic sea ice days is negligibly small, only accounts for 1.6% of the domain-averaged total trend. On the contrary, the thermodynamic component shows coherent decreasing trends over the entire study region among all 12 nodes, which collectively account for 95.8% of the observed August–October Arctic sea ice trend. These coherent decreasing trends are in line with the increases in surface air temperature, total water vapor, and downward longwave radiation over the Arctic Ocean for all 12 nodes, but the spatial relationships between the thermodynamic components and the trends in surface air temperature differ among the 12 nodes. The thermodynamic processes are associated with amplified Arctic warming due to a variety of local feedbacks^{35,38–44}, under the background of the increasing greenhouse gas concentrations.

In our study, the thermodynamic component includes not only the local warming in the Arctic, but also potential changes in the large-scale horizontal gradients of air temperature, air moisture, and sea ice concentration. Even when the occurrence and strength of circulation patterns are unchanged, the atmospheric transports of heat and moisture can change with changing temperature and moisture gradients. In general, the Arctic amplification is expected to result in a weaker meridional gradient

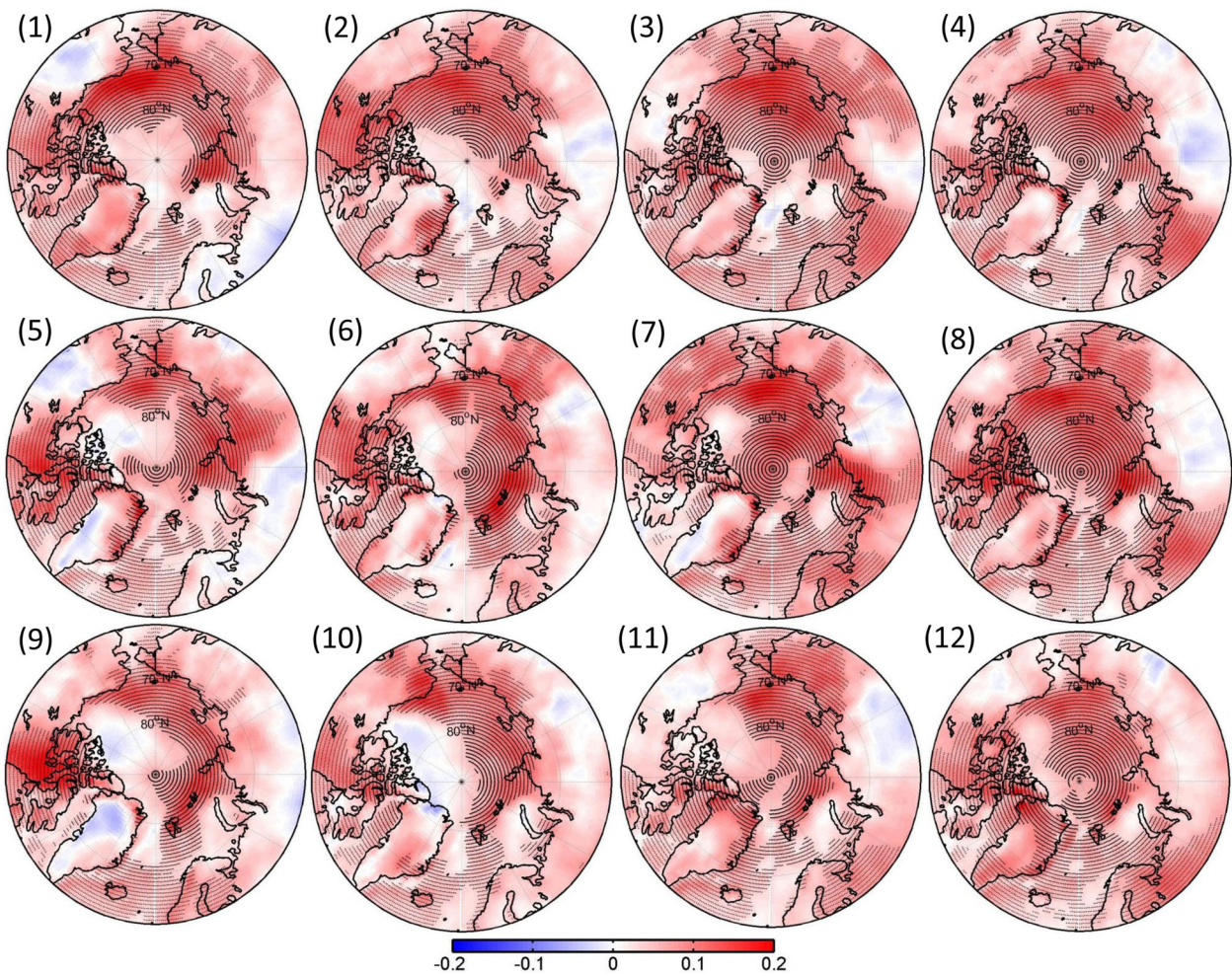


Fig. 10 Trends in surface air temperature for each node (unit: $^{\circ}\text{C yr}^{-1}$).

of air temperature in the mid-high latitudes, but a stronger one in air-specific humidity⁴⁵. This tends to reduce the transport of dry static energy to the Arctic, but increase the transport of latent heat, which enhances the local water vapor and cloud-radiative feedbacks⁴⁶.

Considering the dynamic component, the domain-averaged dynamic trends in sea ice days arise from the effects of changes in the occurrence of 500-hPa level circulation patterns on (a) the atmospheric transport of heat and moisture to the Arctic, (b) oceanic heat transport to the Arctic, and (c) transport of sea ice to warmer waters where it melts. An interesting finding is that, despite the recent rapid sea ice decline in the Arctic, there are also processes that tend to increase sea ice occurrence. These include the positive dynamic components of nodes 9 and 10. These nodes favor large sea ice extent and have become more common during 1979–2016, but their effect is compensated by changes in the occurrence of other nodes.

We have assessed the effect of smaller (4×2 , 3×3) or larger (7×5) SOM grids on spatial patterns. Apart from intra-pattern variability, the SOM grid also influences the changes in the frequency of the SOM node related to dynamic changes. Considering all the nodes, there are two main spatial patterns: the AO and dipole structures. For a smaller SOM grid, the SOM patterns resembling the AO structure would also contain daily patterns with a strongly asymmetric dipole structure, which may strongly influence the variability of Arctic sea ice. For a larger SOM

L. Yu et al.

grid, the important patterns for the sea ice may appear as new node patterns. However, our conclusion that the thermodynamic components dominate the trend in Arctic sea ice loss is independent of the choice of the SOM grid number. In a future study, we shall evaluate the effect of grid number on a study of a particular year, such as 2012, when a strong storm caused a major decline in Arctic summer sea ice extent.

In this study, we concluded that the thermodynamic contribution controls the decadal-scale August–October sea ice loss. Previous studies have shown that spring atmospheric circulation influences the summer sea ice loss in the Arctic^{33,47,48}. The analogous SOM analyses for the April–October period yielded results that are mostly consistent with the results for August to October. However, the spatial patterns of the thermodynamic component have some differences related to the magnitude of the component in the Pacific and Atlantic sectors of the Arctic Ocean. When spring and earlier summer (April–July) are also included in the study period, the relative importance of the Atlantic sector grows.

To summarize, our analyses have demonstrated the dominating role of thermodynamic processes plays in the decline of the August–October (also April–October) Arctic sea ice over the period 1979–2016. Although atmospheric circulation in the Arctic is highly variable, systematic changes in the circulation patterns are small, resulting in overall small dynamic component. However, the atmospheric circulation can contribute to large reduction in sea

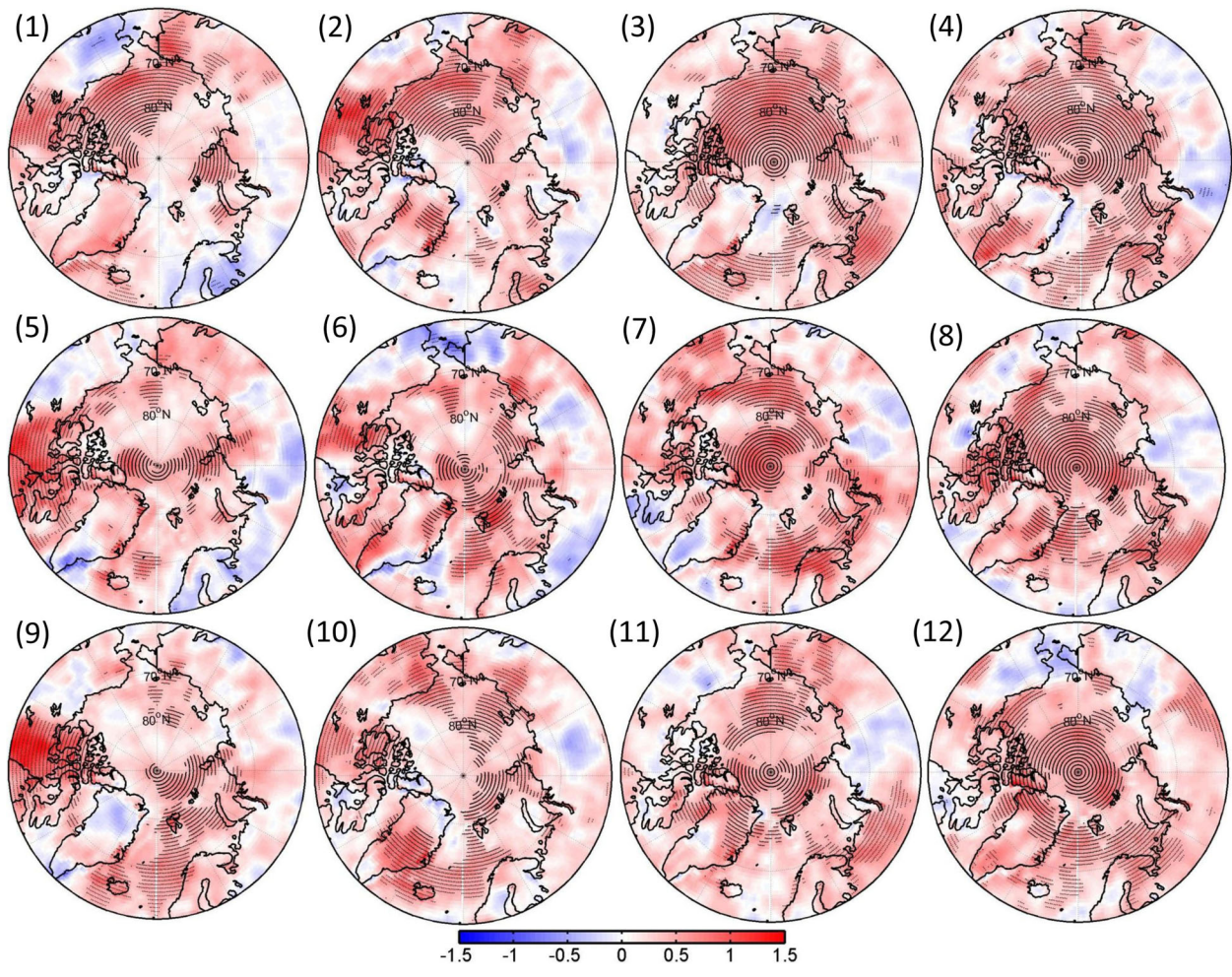


Fig. 11 Trends in surface downward longwave radiation for each node (unit: $\text{W m}^{-2} \text{s yr}^{-1}$).

ice in individual years. For example, atmospheric circulation anomalies played an important role in low sea ice concentrations in the summers of 2007, 2010, 2011, and 2012 (refs. ^{31,48–51}). With a decrease in Arctic sea ice extent, sea ice thickness in the Arctic Ocean has exhibited a strong decrease⁵², which makes the sea ice more vulnerable to atmospheric circulation anomalies.

METHODS

Dataset

The analyses utilize daily sea ice concentration data produced through the National Aeronautics and Space Administration (NASA) Team sea ice algorithm (<https://nsidc.org/data/pm/nasateam-index>) from the U.S. National Snow and Ice Data Center (ftp://sidads.colorado.edu/DATASETS/nsidc0051_gsfc_nasateam_seaice/final-gsfc/north/daily). The sea ice data are archived on a $25 \text{ km} \times 25 \text{ km}$ polar stereographic grid and there are a total of 55,512 grid cells in the study domain. For each grid cell, the number of days with sea ice present, defined as when sea ice occupies at least 15% of the grid cell following Parkinson and Cavalieri⁵³, is determined using the daily sea ice data. This is done for August–October of each year from 1979 through 2016. The months of August through October are selected because they represent the period of strongest sea ice decline in the Arctic Ocean.

Daily fields of 500-hPa geopotential height needed for the analyses are obtained from the ERA-Interim reanalysis dataset⁵⁴ archived on a $1.5^\circ \times 1.5^\circ$ latitude-longitude grid. In addition to the ERA-Interim data, daily AO

index is derived from US Climate Prediction Center (https://www.cpc.ncep.noaa.gov/products/precip/CWlink/daily_ao_index/ao.shtml).

Methods

The primary method used in this study is SOM. The SOM method utilizes a neural-network algorithm with unsupervised learning to reduce a multi-dimensional dataset to a two dimensional array. Each node in the array includes a spatial pattern and the time series of its occurrence frequency. Thus, the array can represent the continuum of the spatial patterns of the dataset. The choice of the number of SOM nodes varies with applications with considerations concerning not only the typical characterization, but also the necessary details in the representation of the spatial patterns of the node^{55,56}. This study uses a 4×3 SOM grid. Larger (e.g., 7×5) or smaller (e.g., 4×2 and 3×3) SOM grids are tested, which yielded similar results to those of the 4×3 SOM grid.

The 4×3 SOM grid is applied to identify the main spatial patterns of daily 500-hPa geopotential height anomalies north of 60°N from August through October during 1979–2016. For each day, a climatological value is obtained by averaging daily data for that day over the 38 years, and an anomaly for that day is obtained by subtracting the climatological value from the daily data.

The SOM method is not new to Arctic climate research. In their pioneering study, SOM method was used to predict changes in net precipitation related to synoptic processes in large Arctic river basins during the 21st century⁵⁷. Other climatological applications of the SOM method have addressed linkages between atmospheric circulation and Arctic sea ice anomalies^{16,58}, atmospheric moisture transport to the Arctic^{47,59} and Antarctic⁶⁰, and impacts of atmospheric large-scale

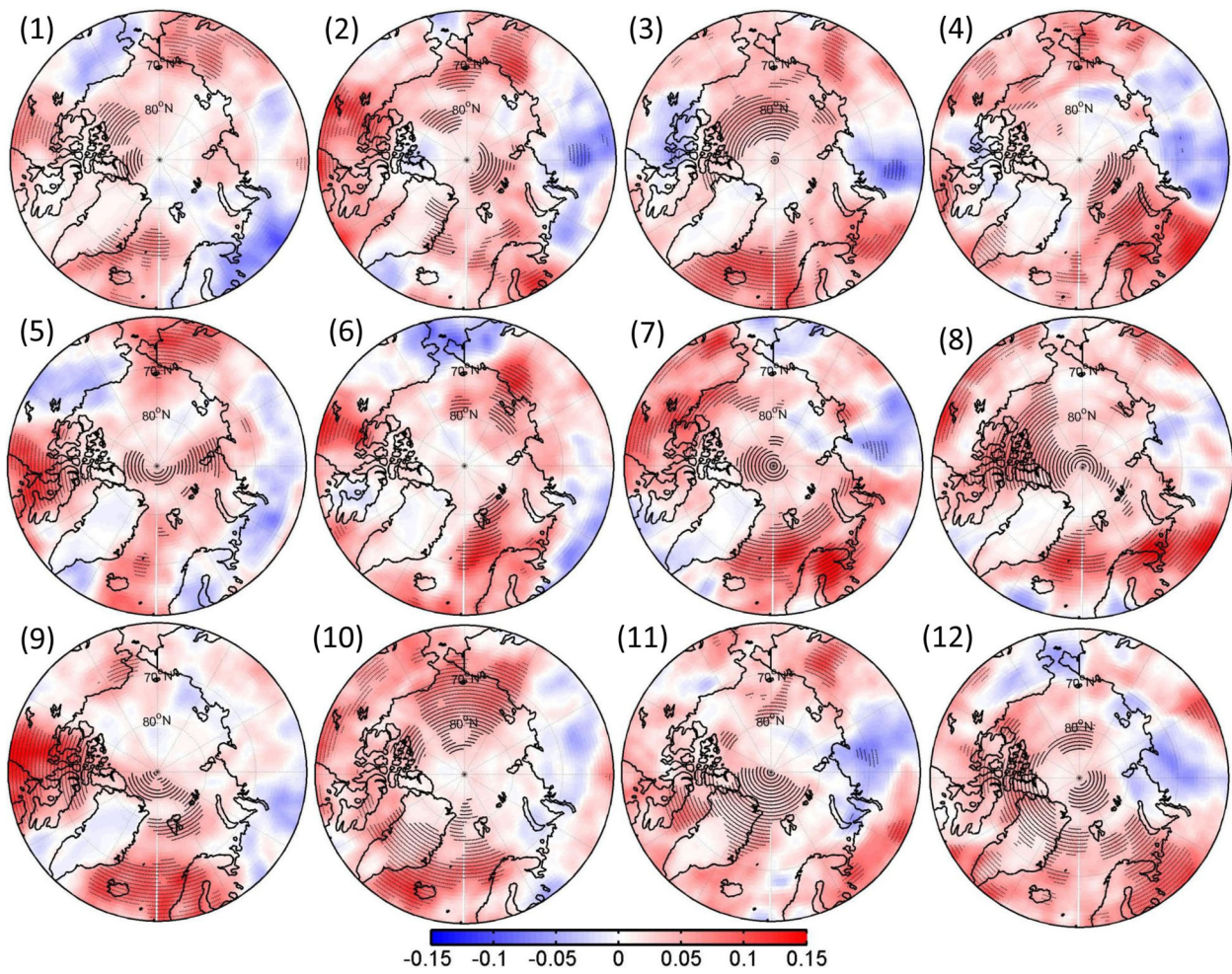


Fig. 12 Trend in total column water vapor for each node (unit: $\text{kg m}^{-2} \text{yr}^{-1}$).

Table 3. Spatial correlation coefficients between the thermodynamic components (Fig. 6) and trends in surface air temperature (Fig. 10) for each node.

	Node 1	Node 2	Node 3	Node 4	Node 5	Node 6	Node 7	Node 8	Node 9	Node 10	Node 11	Node 12
Trend	-0.76	-0.66	-0.51	-0.51	-0.72	-0.74	-0.58	-0.71	-0.61	-0.63	-0.57	-0.59

circulation on mid-latitude temperatures⁶¹. When SOMs are used to cluster atmospheric circulation patterns to study their impact on trends of some other variable, changes in circulation patterns are considered dynamic contributions to the trends, while changes in factors other than circulation patterns are considered as thermodynamic contribution.

Applying the SOM method, we first obtain the main modes of August–October synoptic-scale atmospheric circulation as represented by the SOM spatial pattern on a 4×3 SOM grid. Based on the minimum Euclidean distance, we assign daily 500-hPa height anomalies to the best matching SOM pattern, and thus obtain the occurrence time series of each node. From there, we continue to quantify, following Cassano et al.⁶², the dynamic and thermodynamic contributions to the trend in the frequency of August–October Arctic sea ice days for each grid cell using

$$E = \sum_{i=1}^K (\bar{E}_i + E'_i)(\bar{f}_i + f'_i) \quad (1)$$

Where f_i is the August–October days when its anomalous synoptic circulation pattern (500 hPa height anomalies) is best represented by the

i th SOM node, and E_i is the percentage of August–October days with sea ice presence in all the days of the i th circulation pattern (i th node). If sea ice is present on all the days under the i th circulation pattern, the percentage is 1, and if no sea ice is present on any of the days under the i th circulation, the percentage is 0. K is the number of SOM nodes ($K = 12$ for the 4×3 SOM grid used here). Bars and primes denote the 38-year average and deviation from it, respectively.

Differentiate Eq. (1) with respective to time yields an equation about trends

$$\frac{dE}{dt} = \sum_{i=1}^K \left[\bar{f}_i \frac{dE'_i}{dt} + \bar{E}_i \frac{df'_i}{dt} + \frac{d(E'_i f'_i)}{dt} \right] \quad (2)$$

The left side of the equation displays the total trend in the frequency of August–October Arctic sea ice days for each grid cell. The three components of the right side denote, respectively, the thermodynamic contribution, dynamic contribution, and contribution from their interactions (or simply from chaotic variations³⁷ to the total trend related to the i th SOM node). Here, we stress that the terms dynamic and thermodynamic do not

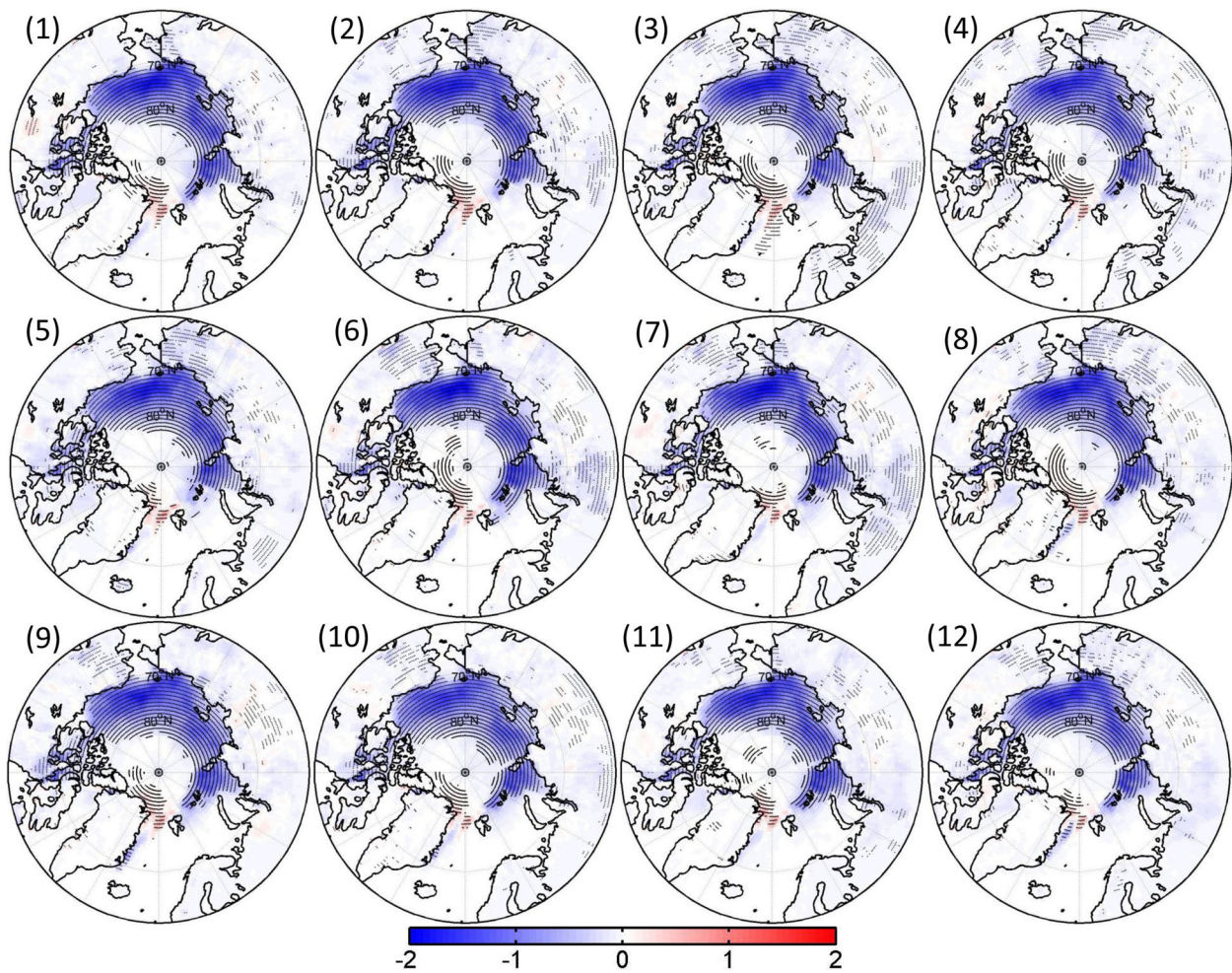


Fig. 13 Trend in albedo for each node (unit: % yr^{-1}).

refer to sea ice dynamics and thermodynamics, but to relationships of between the presence of sea ice and occurrence of various SOM nodes. These relationships are naturally affected by dynamics and thermodynamics of the atmosphere, sea ice, and ocean.

The thermodynamic contribution is calculated by the product of the 38-year average of the SOM pattern occurrence (f_i) and the trend in the percentage of sea ice days per SOM pattern occurrence for each grid cell ($\frac{\partial E}{\partial t}$). The thermodynamic component results from changes in factors controlling occurrence of sea ice under unchanged atmospheric large/synoptic-scale circulation characterized by the SOM nodes. Such factors include decadal-scale trends in air temperature, net radiation on snow/ice surface⁶³, basal melt/growth of sea ice⁶⁴, and increased wind effect on sea ice drift due to thinning of the ice^{32,65}. The dynamic contribution is determined by the product of the trend in the occurrence of SOM patterns ($\frac{df_i}{dt}$) and the 38-year averaged percentage of sea ice days per SOM pattern occurrence (E_i). The dynamic component stems from atmospheric circulation factors associated with the changes in each SOM pattern occurrence. Since we apply daily geopotential height fields, the changes depicted by the SOM nodes include modes of variations at synoptic time scale and beyond. The third component results from the trend of E/f_i , i.e., the product of the anomaly in ice frequency per SOM pattern occurrence and anomaly in the SOM pattern occurrence. Accordingly, a certain SOM pattern contributes positively (negatively) to the so-called interaction component, if there is an increasing (decreasing) trend in simultaneous positive anomalies in the SOM pattern occurrence and sea ice occurrence, or in simultaneous negative anomalies in the SOM pattern occurrence and

sea ice occurrence. Often the so-called interaction component mostly represents internal variability of the system rather than any physical interactions (Sui et al.³⁷),

In addition to our primary study period of August to October, analogous SOM analysis is also carried out for the April–October period to determine if the atmospheric factors controlling decadal trends in sea ice occurrence are different over the spring–summer–early autumn period.

DATA AVAILABILITY

Daily sea ice concentration data produced through the National Aeronautics and Space Administration (NASA) Team sea ice algorithm (<https://nsidc.org/data/pm/nasateam-index>) from the US. National Snow and Ice Data Center (ftp://sidads.colorado.edu/DATASETS/nsidc0051_gsfc_nasateam_seaice/final_gsfc/north/daily).

Daily AO index is derived from US Climate Prediction Center (https://www.cpc.ncep.noaa.gov/products/precip/CWlink/daily_ao_index/ao.shtml). The ERA-Interim data is available from <https://apps.ecmwf.int/datasets/data/interim-full-daily/levtype=sfc/>.

CODE AVAILABILITY

Computer code used to generate results is available upon request.

Received: 18 August 2020; Accepted: 1 December 2020;

Published online: 14 January 2021

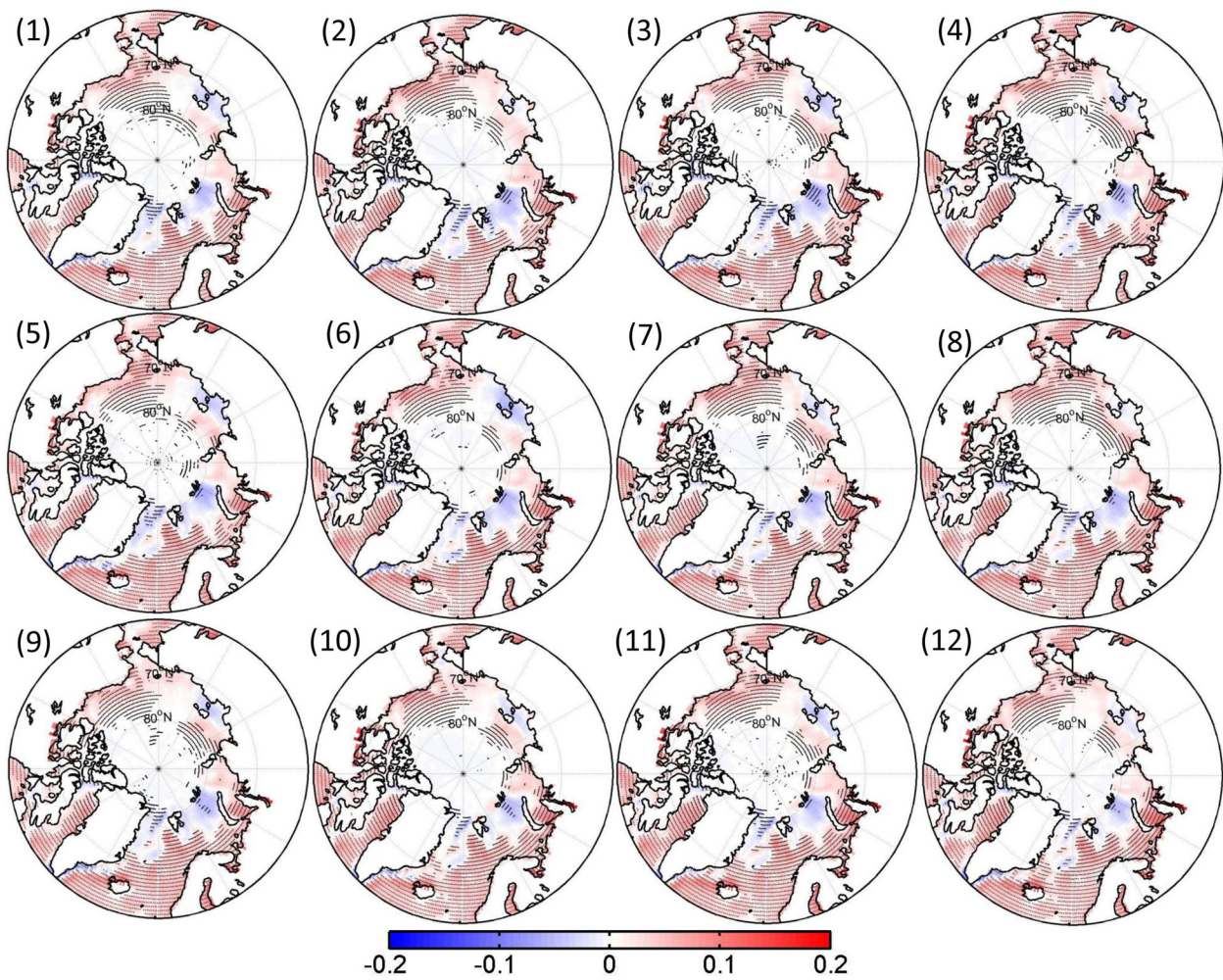


Fig. 14 Trend in sea surface temperature (SST) for each node (unit: $^{\circ}\text{C yr}^{-1}$).

REFERENCES

1. Stroeve, J. C. et al. The Arctic's rapidly shrinking sea ice cover: a research synthesis. *Clim. Change* **110**, 1005–1027 (2012).
2. Gillett, N. P. et al. Attribution of polar warming to human influence. *Nat. Geosci.* **1**, 750–754 (2008).
3. Goosse, H. et al. Quantifying climate feedbacks in polar regions. *Nat. Commun.* **9**, 1919 (2018).
4. Stuecker, M. F. et al. Polar amplification dominated by local forcing and feedbacks. *Nat. Clim. Change* **8**, 1076–1081 (2018).
5. Zhang, J. Warming of the arctic ice-ocean system faster than the global average since the 1960s. *Geophys. Res. Lett.* **32**, L19602 (2005).
6. Min, S.-K., Zhang, X., Zwiers, F. W. & Agnew, T. Human influence on arctic sea ice detectable from early 1990s onwards. *Geophys. Res. Lett.* **35**, 213–236 (2008).
7. Notz, D. & Marotzke, J. Observations reveal external driver for Arctic sea-ice retreat. *Geophys. Res. Lett.* **39**, 89–106 (2012).
8. Gagné, M.-É., Gillett, P. N. & Fyfe, J. C. Impact of aerosol emission controls on future arctic sea ice cover. *Geophys. Res. Lett.* **42**, 8481–8488 (2015).
9. Deser, C., Walsh, J. E. & Timlin, M. S. Arctic sea ice variability in the context of recent atmospheric circulation trends. *J. Clim.* **13**, 617–633 (2000).
10. Rigor, I., Wallace, J. M. & Colony, R. L. Response of sea ice to the Arctic Oscillation. *J. Clim.* **15**, 2648–2663 (2002).
11. Wang, J. et al. Is the Dipole anomaly a major driver to record lows in Arctic summer sea ice extent? *Geophys. Res. Lett.* **36**, L05706 (2009).
12. Woodgate, R. A., Weingartner, T. J. & Lindsay, R. Observed increases in Bering Strait oceanic fluxes from the Pacific to the Arctic from 2001 to 2011 and their impacts on the Arctic Ocean water column. *Geophys. Res. Lett.* **39**, L24603 (2012).
13. Ding, Q. et al. Tropical forcing of the recent rapid Arctic warming in northeastern Canada and Greenland. *Nature* **509**, 209–212 (2014).
14. Zhang, R. Mechanisms for low-frequency variability of summer Arctic sea ice extent. *Proc. Natl Acad. Sci. USA* **112**, 4570–4575 (2015).
15. Yu, L. & Zhong, S. Changes in sea-surface temperature and atmospheric circulation patterns associated with reductions in Arctic sea ice cover in recent decades. *Atmos. Chem. Phys.* **18**, 14149–14159 (2018).
16. Yu, L., Zhong, S., Zhou, M., Lenschow, D. H. & Sun, B. Revisiting the linkages between the variability of atmospheric circulations and Arctic melt-season sea ice cover at multiple time scales. *J. Clim.* **32**, 1461–1482 (2019).
17. Mantua, N. J., Hare, S. R., Zhang, Y., Wallace, J. M. & Francis, R. C. A Pacific interdecadal climate oscillation with impacts on salmon production. *Bull. Am. Meteor. Soc.* **78**, 1069–1079 (1997).
18. Enfield, D. B., Mestas-Nuñez, A. M. & Trimble, P. J. The Atlantic multidecadal oscillation and its relationship to rainfall and river flows in the continental U.S. *Geophys. Res. Lett.* **28**, 2077–2080 (2001).
19. Kay, J. E., Holland, M. M. & Jahn, A. Inter-annual to multi-decadal Arctic sea ice extent trends in a warming world. *Geophys. Res. Lett.* **38**, L15708 (2011).
20. Day, J. J., Hargreaves, J. C., Annan, J. D. & Abe-Ouchi, A. Sources of multi-decadal variability in Arctic sea ice extent. *Environ. Res. Lett.* **7**, 03011 (2012).
21. Ding, Q. A. et al. Fingerprints of internal drivers of Arctic sea ice loss observations and model simulations. *Nat. Geosci.* **12**, 28–33 (2019).
22. Winton, M. Do climate models underestimate the sensitivity of Northern Hemisphere sea ice cover? *J. Clim.* **24**, 3924–3934 (2011).
23. Stroeve, J. C. et al. Trends in Arctic sea ice extent from CMIP5, CMIP3 and observations. *Geophys. Res. Lett.* **39**, L16502 (2012).
24. Mahlstein, I. & Knutti, R. September Arctic sea ice predicted to disappear near 2°C global warming above present. *J. Geophys. Res.* **117**, D06104 (2012).
25. Rosenblum, E. & Eisenman, I. Sea ice trends in climate models only accurate in runs with biased global warming. *J. Clim.* **30**, 6265–6278 (2017).
26. Notz, D. Sea-ice extent and its trend provide limited metrics of model performance. *Cryosphere* **8**, 229–243 (2014).
27. Swart, N. C., Fyfe, J. C., Hawkins, E., Kay, J. E. & Jahn, A. Influence of internal variability on Arctic sea-ice trends. *Nat. Clim. Change* **5**, 86–89 (2015).

28. Notz, D. & Stroeve, J. Observed Arctic sea-ice loss directly follows anthropogenic CO₂ emission. *Science* **354**, 747–750 (2016).
29. Screen, J. A. Arctic sea ice at 1.5 and 2 °C. *Nat. Clim. Change* **8**, 362–363 (2018).
30. Watanabe, E., Wang, J., Sumi, A. & Hasumi, H. Arctic dipole anomaly and its contribution to sea ice export from the Arctic Ocean in the 20th century. *Geophys. Res. Lett.* **33**, L23703 (2006).
31. Ogi, M., Yamazaki, K. & Wallace, J. M. Influence of winter and summer surface wind anomalies on summer Arctic sea ice extent. *Geophys. Res. Lett.* **37**, L07701 (2010).
32. Rampal, P., Weiss, J., Dubois, C. & Campin, J.-M. IPCC climate models do not capture Arctic sea ice drift acceleration: consequences in terms of projected seaice thinning and decline. *J. Geophys. Res.* **116**, C00D07 (2011).
33. Ding, Q. et al. Influence of high-latitude atmospheric circulation changes on summertime Arctic sea ice. *Nat. Clim. Change* **7**, 289–296 (2017).
34. Kohonen, T. *Self-Organizing Maps*, 3rd edn (Springer, New York, 2001).
35. Ramanathan, V. Interactions between ice-albedo, lapse-rate and cloud-top feedbacks: an analysis of the nonlinear response of a GCM climate model. *J. Atmos. Sci.* **34**, 1885–1897 (1977).
36. Vihma, T., Tisler, P. & Uotila, P. Atmospheric forcing on the drift of Arctic sea ice in 1989–2009. *Geophys. Res. Lett.* **39**, L02501 (2012).
37. Sui, C., Yu, L. & Vihma, T. Occurrence and drivers of wintertime temperature extremes in Northern Europe during 1979–2016. *Tellus A* **72**, 1788368 (2020).
38. Wetherald, R. T. & Manabe, S. Cloud feedback processes in a general circulation model. *J. Atmos. Sci.* **45**, 1397–1415 (1988).
39. Bitz, C. M. & Roe, G. H. A mechanism for the high rate of sea ice thinning in the Arctic Ocean. *J. Clim.* **17**, 3623–3632 (2004).
40. Bintanja, R., Graversen, R. G. & Hazelger, W. Arctic winter warming amplified by the thermalinversion and consequent low infrared cooling to space. *Nat. Geosci.* **4**, 758–761 (2011).
41. Flanner, M. G., Shell, K. M., Barlage, M., Perovich, D. K. & Tschudi, M. A. Radiative forcing and albedo feedback from the Northern Hemisphere cryosphere between 1979 and 2008. *Nat. Geosci.* **4**, 151–155 (2011).
42. Sedlar, J. et al. A transitioning Arctic surface energy budget: the impacts of solar zenith angle, surface albedo and cloud radiative forcing. *Clim. Dyn.* **37**, 1643–1660 (2011).
43. Gordon, N. D., Jonko, A. K., Forster, P. M. & Shell, K. M. An observationally based constraint on the water-vapor feedback. *J. Geophys. Res. Atmos.* **118**, 12435–12443 (2013).
44. Pitman, F. & Mauritzen, T. Arctic amplification dominated by temperature feedbacks in contemporary climate models. *Nat. Geosci.* **7**, 181–184 (2014).
45. Hwang, Y.-T., Frierson, D. M. W. & Kay, J. E. Coupling between Arctic feedbacks and changes in poleward energy transport. *Geophys. Res. Lett.* **38**, L17704 (2011).
46. Graversen, R. G. & Wang, M. Polar amplification in a coupled climate model with locked albedo. *Clim. Dyn.* **33**, 629–643 (2009).
47. Kapsch, M.-L., Skific, N., Graversen, R. G., Tijernstrom, M. & Francis, J. A. Summer with low Arctic sea ice linked to persistence of spring atmospheric circulation patterns. *Clim. Dyn.* **52**, 2497–2512 (2019).
48. Ogi, M., Rigor, I. G., McPhee, M. G. & Wallace, J. M. Summer retreat of Arctic sea ice: Role of summer winds. *Geophys. Res. Lett.* **35**, L24701 (2008).
49. Ogi, M. & Wallace, J. M. Summer minimum Arctic sea-ice extent and the associated summer atmospheric circulation. *Geophys. Res. Lett.* **34**, L12705 (2007).
50. Ogi, M. & Wallace, J. M. The role of summer surface wind anomalies in the summer Arctic sea ice extent in 2010 and 2011. *Geophys. Res. Lett.* **39**, L09704 (2012).
51. Simmonds, I. & Rudeva, I. The great arctic cyclone of August 2012. *Geophys. Res. Lett.* **39**, L23709 (2012).
52. Kwok, R. Arctic sea ice thickness, volume, and multiyear ice coverage: losses and coupled variability (1958–2018). *Environ. Res. Lett.* **13**, 105005 (2018).
53. Parkinson, C. L. & Cavalieri, D. J. Arctic sea ice variability and trends, 1979–2006. *J. Geophys. Res.* **113**, C07003 (2008).
54. Dee, D. P. et al. The ERA-Interim reanalysis: configuration and performance of the data assimilation system. *Quart. J. Roy. Meteor. Soc.* **137**, 553–597 (2011).
55. Cassano, J. J., Uotila, P., Lynch, A. H. & Cassano, E. N. Predicted changes in synoptic forcing of net precipitation in large Arctic river basins during the 21st century. *J. Geophys. Res.* **112**, G04S49 (2007).
56. Johnson, N. C. & Feldstein, S. B. The continuum of North Pacific sea level pressure patterns: intraseasonal, interannual, and interdecadal variability. *J. Clim.* **23**, 851–867 (2010).
57. Lee, S. & Feldstein, S. B. Detecting ozone- and greenhouse gas-driven wind trends with observational data. *Science* **339**, 563–567 (2013).
58. Lynch, A. H., Serreze, M. C., Cassano, E. N., Crawford, A. D. & Stroeve, J. Linkages between Arctic summer circulation regimes and regional sea ice anomalies. *J. Geophys. Res. Atmos.* **121**, 7868–7880 (2016).
59. Nygård, T., Graversen, R. G., Uotila, P., Naakka, T. & Vihma, T. Strong dependence of wintertime Arctic moisture and cloud distributions on atmospheric large-scale circulation. *J. Clim.* **32**, 8771–8790 (2019).
60. Yu, L. et al. Features of extreme precipitation at Progress station, Antarctica. *J. Clim.* **31**, 9087–9105 (2018).
61. Vihma, T. et al. Effects of the tropospheric large-scale circulation on European winter temperatures during the period of amplified Arctic warming. *Int. J. Climatol.* **40**, 509–529 (2020).
62. Cassano, J. J., Uotila, P., Lynch, A. H. & Cassano, E. N. Predicted changes in synoptic forcing of net precipitation in large Arctic river basins during the 21st century. *J. Geophys. Res.* **112**, G04S492007 (2007).
63. Gong, T., Feldstein, S. & Lee, S. The role of downward infrared radiation in the recent Arctic winter warming trend. *J. Clim.* **30**, 4937–4949 (2017).
64. Stroeve, J. C., Markus, T., Boisvert, L., Miller, J. & Barrett, A. Changes in Arctic melt season and implications for sea ice loss. *Geophys. Res. Lett.* **41**, 1216–1225 (2014).
65. Vihma, T. et al. Advances in understanding and parameterization of small-scale physical processes in the marine Arctic climate system: a review. *Atmos. Chem. Phys.* **14**, 9403–9450 (2014).

ACKNOWLEDGEMENTS

This study is supported by National Key R&D Program of China (Numbers: 2017YFE0111700 and 2019YFC1509102) and the National Natural Science Foundation of China (41922044). The work of Timo Vihma was supported by the Academy of Finland (contract 317999). We thank ECMWF for offering ERA-Interim reanalysis.

AUTHOR CONTRIBUTIONS

L.Y. designed the story line, analyzed the data, and wrote the draft. S.Z. and T.V. were equally contributed in writing and revising of the paper. B.S. offered the revised suggestion.

COMPETING INTERESTS

The authors declare no competing interests.

ADDITIONAL INFORMATION

Supplementary information is available for this paper at <https://doi.org/10.1038/s41612-020-00157-4>.

Correspondence and requests for materials should be addressed to L.Y.

Reprints and permission information is available at <http://www.nature.com/reprints>

Publisher's note Springer Nature remains neutral with regard to jurisdictional claims in published maps and institutional affiliations.



Open Access This article is licensed under a Creative Commons Attribution 4.0 International License, which permits use, sharing, adaptation, distribution and reproduction in any medium or format, as long as you give appropriate credit to the original author(s) and the source, provide a link to the Creative Commons license, and indicate if changes were made. The images or other third party material in this article are included in the article's Creative Commons license, unless indicated otherwise in a credit line to the material. If material is not included in the article's Creative Commons license and your intended use is not permitted by statutory regulation or exceeds the permitted use, you will need to obtain permission directly from the copyright holder. To view a copy of this license, visit <http://creativecommons.org/licenses/by/4.0/>.

© The Author(s) 2021

© The Author(s) 2021. This work is published under
<http://creativecommons.org/licenses/by/4.0/>(the “License”). Notwithstanding
the ProQuest Terms and Conditions, you may use this content in accordance
with the terms of the License.